

Evaluation and Simulation of SAR Among Patients Using MRI Machines

Adel Saad. Emhemmed
*Electrical and Electronics Engineering
Department
University of Tripoli
Tripoli, Libya
dr.adel.elec@gmail.com*

Ibrahim Asaad Aref
*School of Computing and
Communications
Lancaster University
Lancaster, UK
i.aref@lancaster.ac.uk*

Mahmoud Khaled Elbezanti
*Electrical and Electronics Engineering
Department
University of Tripoli
Tripoli, Libya*

Majed Hisham Gmati
*Electrical and Electronics Engineering
Department
University of Tripoli
Tripoli, Libya*

Abstract— The expanding use of electric devices in everyday life has led to an augmented interest in investigating the interaction between electromagnetic fields and biological tissues. In order to ensure the secure advancement of electromagnetic devices and avoid potential health hazards, comprehending the distribution of electromagnetic fields in the human body is imperative. Magnetic resonance imaging (MRI) is a widely accepted technique for medical diagnosis. The use of high-field MRI has become increasingly popular in recent years as it can enhance signal-to-noise ratio (SNR) and image resolution, thereby decreasing acquisition time. This paper aims to investigate the impact of electromagnetic waves on the human body, particularly the specific absorption rate (SAR). Accurately calculating SAR in humans poses significant challenges and requires advanced mathematical models and computer simulations. To this end, the study utilized the Microwave Studio Transient Solver available in CST Studio Suite 2020 to solve the electromagnetic problem in different human models.

Keywords— *Magnetic resonance imaging, SAR, Simulation, CST.*

I. INTRODUCTION

With the increase in the use of electric appliances in daily life, there is growing interest in studying the interaction of electromagnetic fields with biological tissues. To ensure the safe development of electromagnetic devices and prevent any potential health risks, it is crucial to understand the distribution of electromagnetic fields in the human body. However, direct measurement of the electromagnetic fields inside living tissues and organs is challenging [1]. Fortunately, with the rapid development of computer technology, simulations using human body models can be utilized to predict the effects of electromagnetic radiation, including heating and the Specific Absorption Rate (SAR) distribution.

Magnetic resonance imaging (MRI) is widely used for medical diagnosis, with high-field MRI gaining popularity in recent years due to its ability to improve signal-to-noise ratio (SNR) and image resolution, leading to reduced acquisition time. However, as the use of high-field MRI becomes more common, ensuring patient safety is a growing concern [2]. One significant risk during MRI scanning is the potential heating of metallic medical implants due to the absorption of radiofrequency (RF) energy. The degree of risk is influenced

by various factors, including RF power, static magnetic field strength, implant shape and location, as well as pulse sequences and imaging parameters. Accurate measurement of the specific absorption rate (SAR) of RF energy absorbed by the body is crucial, with international standards requiring that average SAR values do not exceed 4 W/kg for the body and 3.2 W/kg for the head over a duration of 6 minutes. The U.S. Food and Drug Administration has further limited average SAR values to 3 W/kg for head scans lasting 10 minutes and 4 W/kg for body scans lasting 15 minutes. Local SAR levels averaged over 10 g of tissue also require restriction, even if a higher level is permissible. The American Society for Testing and Materials (ASTM) has developed technical standards for evaluating RF heating due to passive implantable medical devices during MRI scans [2,3].

MRI scanners estimate SAR levels based on various factors, but these values may not be accurate, especially when metal implants are present. Numerical simulations of RF energy deposition in anatomical models have been used to predict SAR levels, but these models have limitations. There is a need for an independent tool to measure SAR values and verify the power level. The Microwave Studio Transient Solver within CST Studio Suite 2020 (Computer Simulation Technology) was used to solve the electromagnetic problem on several human models, a 1.5T and 3T MRI models were used and the SAR distributions within the tissue models averaged over the whole body over one gram, and locally over ten grams of tissue were calculated [3-6]. The main aim of this work is to study the effect of electromagnetic waves on the patient's body, which is known as the specific absorption rate. Precise calculation of SAR in humans is challenging, and it requires sophisticated mathematical models and computer simulations. This work employed the Microwave Studio Transient Solver in CST Studio Suite 2020 to solve the electromagnetic problem in various human models. The SAR distributions in tissue models were calculated by averaging over the whole body and locally over ten grams of tissue for 1.5T and 3T MRI models.

II. MAGNETIC RESONANCE IMAGING

Magnetic resonance imaging (MRI) is a non-invasive imaging modality that provides detailed three-dimensional anatomical images and is commonly used for disease detection, diagnosis, and therapy monitoring. This technique

is based on the stimulation and detection of changes in the rotational axis of protons within water molecules in living tissues, utilizing state-of-the-art technology.

A magnetic field and radio frequency (RF) impulses are used in magnetic resonance imaging (MRI), which produces pictures of anatomical structures inside the human body. Images created by MRI machines are noticeably different from those created by other imaging modalities. The ability of the MRI method to selectively photograph a variety of tissue properties is one of the main differences. If a pathologic process affects multiple tissue properties without altering just one and producing contrast, it may still be evident in an image due to its impact on other qualities. This makes the MRI process a little more difficult than other imaging techniques. The user must have a thorough understanding of the properties of the Magnetic Resonance Image (MRI) and how its characteristics can be adjusted in order to optimize an MRI process for a particular clinical assessment [3-6].

The MRI system is composed of a number of subnetworks, each of which contributes to the capability required to produce images of an object. The MRI's components are displayed in Figure 3-6. The fundamental elements of every MRI system are: The main magnet, essential for achieving equilibrium and spin alignment. Image encoding in the x, y, and z axes is made possible using gradient coils (ie, the frequency, phase, and slice encoding directions). The component of the MRI system known as the RF coil is responsible for exciting the aligned spins and receiving an RF signal from the sample. Through a console, the user can control and interact with every component. Figure 1 depicts the MRI image that was produced [3].

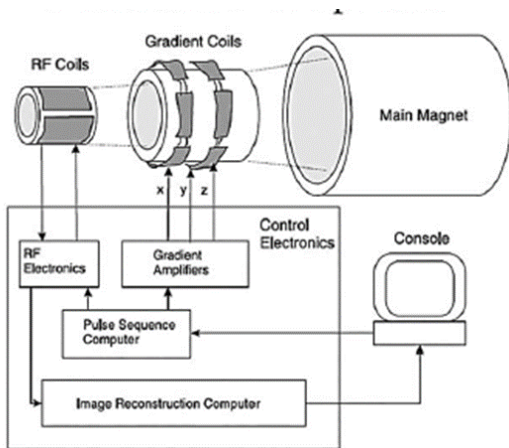


Fig. 1 MRI scanner components

The two main MRI machine types are closed MRI and open MRI. Open bore MRI machines, which lack an enclosed environment, may offer more comfort during imaging even though closed bore MRI machines produce the highest-quality images[2].

III. SIMULATION AND RESULTS

In this section, the specific absorption rate generated by an MRI machine has been studied and analyzed on several human models, including a man, woman, child, and newborn using CST software.

The CST design environment is a user-friendly interface that is utilized by all modules. It includes a 3D interactive modelling tool, a schematic layout tool, a pre-processor for the

electromagnetic solvers, and post-processing tools designed to meet the specific needs of the industry.

The MRI model consists of a cylindrical shield and a typical bird-cage coil and lumped capacitors. The coil is driven by two discrete ports positioned at a 90° angle, which excites the required rotating field [4]. Figure 4-2 Shows the MRI model used in this project.

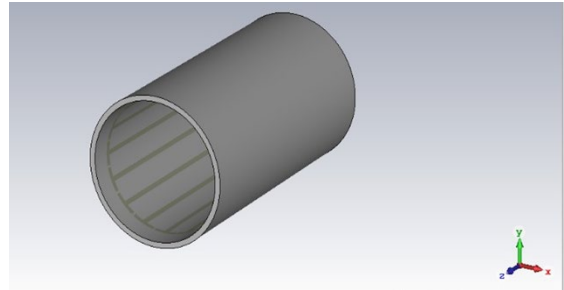


Fig. 2 MRI Model

A. Human Models

The CST Voxel Family comprises seven human models with varying sizes, ages, and genders, as depicted in Figure 3. These models are derived from the GSF voxel family created by Helmholtz Zentrum München-Deutsches Forschungszentrum für Gesundheit und Umwelt[5,6]. The human models are developed from CT and MR images of patients and consist of up to 135 tissues and organs distributed across 2-5 million voxels. Figure 4 presents a frontal and side view of the human organs. These models have broad applications, including simulations of ionizing radiation exposure, radiation therapy, and others. For this project, the Baby, Child, Gustav, and Laura models were utilized. The characteristics of the CST voxel family models are shown in Table I.

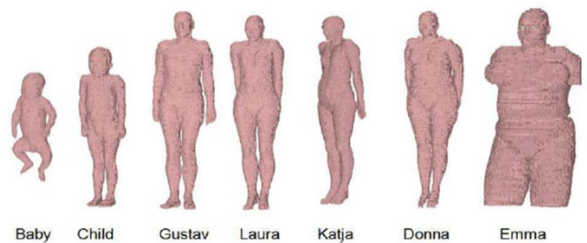


Fig. 3 CST Voxel Family



Fig. 4 Human body organs

TABLE I. CST VOXEL FAMILY CHARACTERISTICS

Model	Age	Sex	Size (cm)	Mass (kg)	Resolution/mm
Baby	8wks	Female	57	4.2	0.85× 0.85× 4.0
Child	7yrs	Female	115	21.7	1.54× 1.54× 8.0
Donna	40yrs	Female	176	79	1.875× 1.875× 10.0
Emma	26yrs	Female	170	81	0.98× 0.98× 10.0
Gustav	38yrs	Male	176	69	2.08× 2.08× 8.0
Laura	43yrs	Female	163	51	1.875× 1.875× 5.0
Katja	43yrs	F-pregnant	163	62	1.775× 1.775× 4.84

B. SAR Simulation

The human models shown above were simulated in 1.5 Tesla and 3 Tesla MRI machines to show the difference in the specific absorption rate in both cases.

IV. SAR SIMULATION

The human models shown above were simulated in 1.5 Tesla and 3 Tesla MRI machines to show the difference in the specific absorption rate in both cases.

A. Simulation of 1.5T MRI

First, a 1.5T MRI machine was simulated to study the SAR of every human model, the SAR results are shown in Table II, SAR was calculated according to two standards: the 1g standard and the 10g standard.

TABLE II. 1.5T SAR VALUES FOR 1G AND 10G STANDARDS

Model	SAR(1g) [w/kg]	SAR(10g) [w/kg]
Gustav	1.42	0.916
Laura	0.937	0.641
Child	0.445	0.293
Baby	0.427	0.268

The SAR distribution for each model used is shown in the following figures. First a male (Gustav) human model was simulated, the SAR distribution is shown in Figure 5.

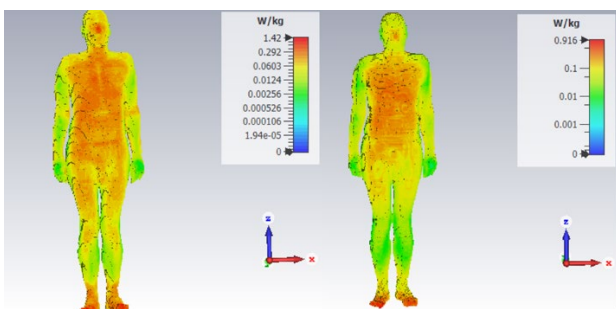


Fig. 5: Gustav SAR distribution in 1.5T MRI for : (a) 1g , (b) 10g

Figure 6 displays the SAR distribution for the female human model (Laura). The child's SAR distribution is shown in Figure 7, while Figure 8 illustrates the newborn (baby) SAR distribution.

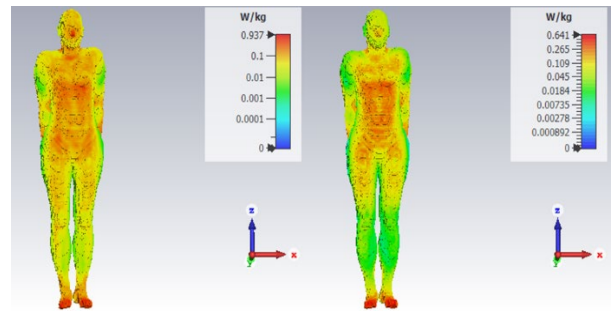


Fig. 6: Laura SAR distribution in 1.5T MRI for : (a) 1g , (b) 10g

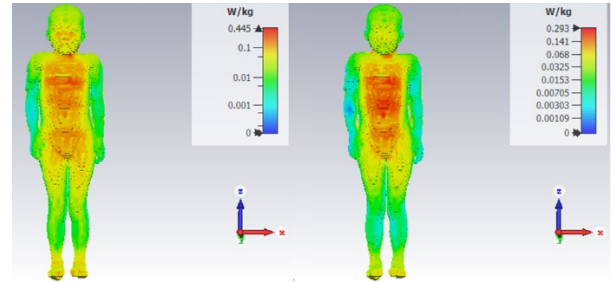


Fig. 7: Child SAR distribution in 1.5T MRI for : (a) 1g , (b) 10g

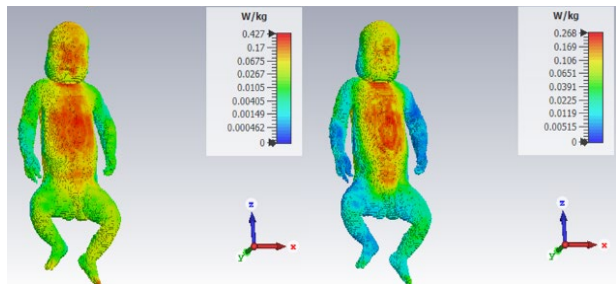


Fig. 8: Baby SAR distribution in 1.5T MRI for : (a) 1g , (b) 10g

From the results in Table II, the SAR value is lower in neonates (baby) than the other human models under equivalent RF conditions, and as seen from the previous figures, the SAR distributions were variable and the peak SAR values generally occurred in the chest area.

B. Simulation of 3T MRI

The SAR of each human model was examined using a 3T MRI simulator; the findings are displayed in Table 4.3. The SAR was determined also using two standards: the 1g standard and the 10g standard.

TABLE III. 3T SAR VALUES FOR 1G AND 10G STANDARDS

Model	SAR(1g) [w/kg]	SAR(10g) [w/kg]
Gustav	2.21	1.77
Laura	2.13	1.49
Child	1.76	0.768
Baby	1.29	0.691

The following figures display the SAR distribution for each of the utilized models. First a male (Gustav) human

model was simulated, the SAR distribution is shown in figure 9.

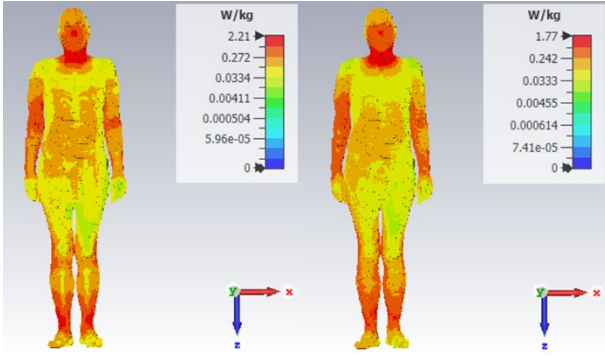


Fig. 9: Gustav SAR distribution in 3T MRI for : (a) 1g , (b) 10g

Figure 10 displays the SAR distribution for the female human model (Laura).

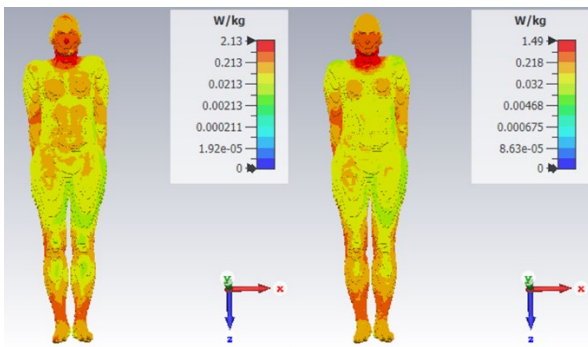


Figure 10: Laura SAR distribution in 3T MRI for : (a) 1g , (b) 10g

The child's SAR distribution is shown in Figure 11.

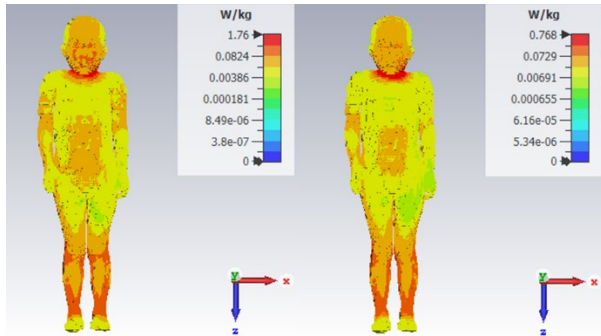


Fig. 11: Child SAR distribution in 3T MRI for : (a) 1g , (b) 10g

Figure 12 illustrates the newborn (baby) SAR distribution.

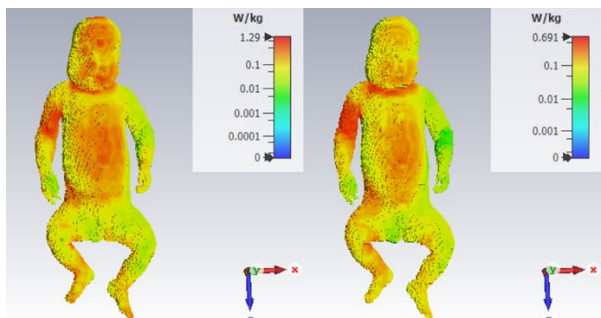


Fig. 12: Baby SAR distribution in 3T MRI for : (a) 1g , (b) 10g

As shown in Table 4, the SAR values were in the same order when using 1.5T MRI but at higher levels, and due to the final equation for calculating the SAR, it was higher at the 1 gram standard than at 10 grams.

C. 1.5T Simulation of Human Organs

In this section, selected human organs were simulated at 1.5T to show which organ is the most affected by MRI scans, the organs chosen were the heart, brain lungs and liver. The SAR values of each organ are shown in Table IV

TABLE IV. SAR VALUES OF SOME HUMAN ORGANS

Organ	SAR(1g) [w/kg]
Lungs	0.872
Brain	0.215
Liver	0.135
Heart	0.105

The SAR distribution of each organ is shown in the following figures.

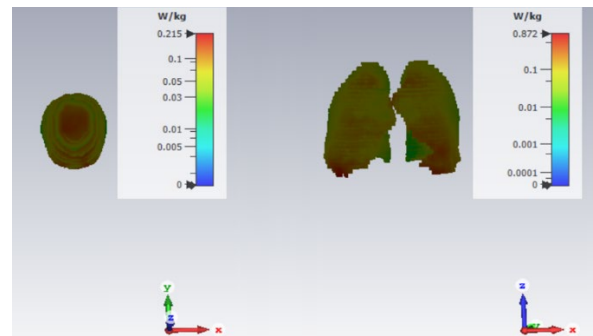


Fig. 13: SAR distribution on : (a) Brain. (b) Lungs

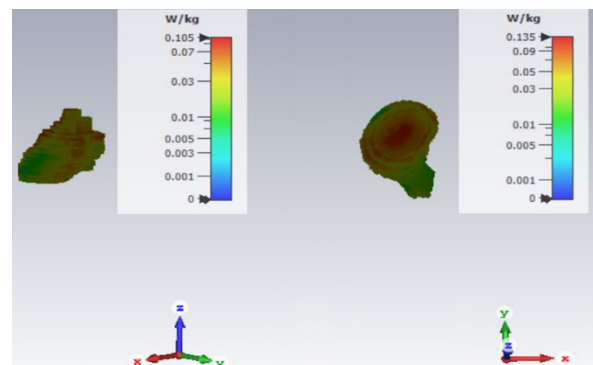


Fig. 14: SAR distribution on : (a) Heart. (b) Liver

According to table 4.4 findings, the lung's SAR value is higher than that of other human organs under the same conditions. The distribution of SAR was nearly uniform in the lungs and heart, while in both the brain and liver it peaked at the center as shown in figure 13 and figure 14.

D. Actual SAR and measured SAR comparison

To compare the simulation SAR and actual SAR from a physical MRI machine a hospital and a medical imaging center were visited to obtain a SAR reading, the Tripoli central hospital which uses a Philips ingenia 1.5T and Alekhtyar Alafdal medical imaging center which uses a GE signa explorer, the results are compared with the male (Gustav) human model (1g).

In the 1.5T simulation the measured SAR is equal to 1.42 W/Kg, the Tripoli central hospital result is equal to 2.5 W/Kg while the Alekhtyar Alafdal medical imaging center result is equal to 2.02 W/Kg. as shown all the results differ slightly mainly due to the difference in weight between the human model and the patients and the difference in hardware.

V. CONCLUSION

MRI has developed into a vital diagnostic and monitoring tool for patients, and its diagnostic standards have consistently improved to make them more practical and user-friendly. However, when taking an MRI scan the specific absorption rate (SAR) should be observed in order not to exceed standard limits, The SAR quantifies the extent to which the patient's tissue may heat up as a result of the RF energy needed for generating the MR signal.

The specific absorption rate increases with body mass, the male (Gustav) model has the highest SAR (1.42 W/Kg) and highest mass (69 Kg) compared to the other models Therefore smaller patients have a lower risk of tissue heating. In addition, The specific absorption rate increases with operating

frequency, the 3T SAR readings of the models such as Female (Laura) with SAR value of 2.13 W/Kg is greater than the 1.5T reading of 0.937 W/Kg, Therefore 1.5T MRI scanners are safer than 3T MRI scanners.

The highest SAR value obtained from the simulation was 1.42w/kg for a 1.5T MRI. This value is within the safe range according to the FDA SAR limits. Also each of the readings obtained during the visit to the Tripoli central hospital and Alekhtyar Alafdal medical imaging center was within the safe range for the imaging process.

REFERENCES

- [1] Wlad T. Sobol, "Recent advances in MRI technology: Implications for image quality and patient safety", Saudi J Ophthalmol ,2012 Oct.
- [2] T. S. Ibrahim and R. Lee, "Evaluation of MRI RF probes utilizing infrared sensors", IEEE Trans. Biomed. Eng., vol. 53, no. 5, pp. 963-967, May 2006.
- [3] Yanasak, J. A. (2015). What MRI Sequences Produce the Highest Specific Absorption Rate (SAR), and Is There Something We Should Be Doing to Reduce the SAR During Standard Examinations? American Journal of Roentgenology , W140.
- [4] "CST Studio Suite 3D EM simulation and analysis software", DASSAULT SYSTEMS. [online] <https://www.3ds.com/products-services/simulia/products/cst-studio-suite/> (accessed Sep, 9, 2022).
- [5] N. Petoussi-Henss, M. Zankl, U. Fill, and D. Regulla, "The GSF family of voxel phantoms," Physics in Medicine and Biology, Neuberberg, Germany, 2002.
- [6] M. Zankl, N. Petoussi-Henss, U. Fill, and D. Regulla, "The application of voxel phantoms to the internal dosimetry of radionuclides," Radiation Protection Dosimetry, vol. 105, 2003.